RSC Advances

ROYAL SOCIETY OF CHEMISTRY

www.rsc.org/advances

The Suitability of Ce^{3+} modified ZnO Photocatalyst for the mineralization of monochlorophenol isomers in sunlight exposure

Mohammad Aslam[1], Iqbal M. I. Ismail[1,2], Sivaraman Chandrasekaran[1], Talal Almeelbi[1,3] and Abdul Hameed[1, 4*]

[1]Centre of Excellence in Environmental Studies (CEES), King Abdulaziz University, Jeddah 21589, Saudi Arabia.

[2]Chemistry Department, Faculty of Science, King Abdulaziz University, Jeddah 21589, Saudi Arabia.

[3]Department of Environmental Sciences, King Abdulaziz University, Jeddah 21589, Saudi Arabia.

[4]National Centre for Physics, Quaid-e-Azam University, Islamabad 44000, Pakistan.

[*]**Corresponding Author:** afmuhammad@kau.edu.sa

Key words: Sunlight photocatalysis, chlorophenol, ZnO, Ce^{3+} surface modification

Abstract

The photocatalytic activity of Ce^{3+} modified hexagonal ZnO for the degradation / mineralization of monochlorophenol isomers (*2-chlorophenol, 3-chlorophenol and 4-chlorophenol)*, in natural sunlight exposure, is reported. Compared to bare ZnO, The modified catalysts showed superior activity for the mineralization of MCP isomers. The identification of the intermediates disclosed that the mode of degradation of chlorophenol substrates also varies with increased Ce^{3+} loading. Increased mineralization was discovered with increasing concentration of Ce^{3+} at the surface of ZnO. The correlation of the results obtained by various analytical tools divulged that the photocatalytic removal of MCP isomers initially proceeds with the cleavage of the aromatic ring, release of chloride ions and formation of oxygenated intermediates. The intermediates are oxidized further by the oxidizing species to mineralization finally. The efficacy of the synthesized catalysts was tested for the mixture of chlorophenol isomers. Based on the intermediates formed, the major contribution of superoxide anion radicals was evidenced in the removal process. The Ce^{3+} impregnation protected the surface of ZnO against photocorrosion.

Introduction

The hazards and toxicity of chlorophenols, even in a very low concentration, are well established.[1-7] The petrochemical and pesticide industries are spotted as the major sources of chlorophenol polluted industrial wastewater. On the other hand, the excessive use of chlorophenols as sanitizers contributes in contaminating the domestic wastewater. Additionally, the formation of chlorophenols during the disinfection of water is also documented as a potential source.[5-10]

The chemical stability and transformation of chlorophenols into more toxic intermediates hinders their large scale and efficient removal from the wastewater by chemical and biological methods.[9,10] Adsorption is viewed as a viable approach in this contest, however; storage and disposal of the large quantities of adsorbent loaded with toxic chlorophenols questions the large-scale use of this technology.[10-15]

The light mediated generation of highly reactive oxidizing radicals for the oxidation of toxic pollutant label the advanced oxidation processes as cheap, efficient and environmental friendly processes.[16-18] Among these, heterogeneous photocatalysis is a versatile approach as it is associated with the complete conversion of organic carbon to CO_2 without leaving any secondary intermediate. The affluent availability of nontoxic photocatalysts, such as TiO_2 and ZnO, makes this approach more attractive for environmental remediation, especially decontamination of water.[19-27]

TiO_2 was found to be the most studied photocatalyst for the degradation of chlorophenols and the researchers have proposed the mechanism of photocatalytic degradation of chlorophenols based on their experiments.[21,28-35] The principal pathway for the photocatalytic degradation of chlorophenols is through its interaction of hydroxyl radicals, which is produced during the course of the photocatalytic reaction. The position of chlorine atoms in the chlorophenols was reported to play a significant role in the formation of the intermediate compounds during the course of reaction.[36] Pyrocatechol was formed as an intermediate compound when 2-chlorophenol subjected to photocatalytic degradation, whereas resorcinol formed in 3-chlorophenol and in case of 4-chlorophenol it resulted in the generation of a mixture of intermediates such as

hydroquinone, benzoquinone and benzenetriol.[37-39] It was widely being reported in the literature that degradation pathways, product yields and reaction rates strongly depend on the photocatalytic reaction conditions.[40]

ZnO, with the bandgap of 3.2 eV, is an important substitute of TiO_2 and sometimes preferred due to its higher photon absorption cross section.[41,42] However, the ZnO suffers the problems of fast recombination rate and low stability against photo-corrosion. It is well established that the photocatalytic activity and the chemical stability of a photocatalyst can be enhanced by modifying its surface.[20,43,44]

Being renewable, the use of sunlight as an excitation source for the generation of highly energetic reactive radicals, for the mineralization of organic contaminants, is a conspicuous option and can expand the scope of this technology. However, the non-availability of sunlight active photocatalysts limits the use of this cheap natural photon source in photocatalysis. Therefore, for the future and widespread commercial use of this technology, it is highly desired to develop either new sunlight responsive, active photocatalysts or to modify the existing active photocatalysts for better sunlight response. Various strategies are reported in the literature to make the existing active photocatalysts such as TiO_2 and ZnO, responders in the visible region. These strategies include metal ion doping, composite formation, surface modification by metal impregnation and insertion of non-metals such as S and N.

We have recently reported the synthesis, characterization and preliminary results regarding the enhanced photocatalytic activity of Ce^{3+} impregnated ZnO photocatalysts for the degradation of 2-chlorophenol (2-CP) as short communication.[45] The present study is a detailed investigation of the photocatalytic activity of a series of synthesized catalysts with different loading of Ce^{3+} (0.5%, 1%, 3%, 5% and 10%) in the natural sunlight for the degradation/mineralization of individual monochlorophenol (MCP) isomers initially and to a mixture of these isomers finally. HPLC and TOC were affianced for estimating the progress of degradation and mineralization process. Ion chromatography measured the ions released during the course of photocatalytic process, while GC-MS identified the intermediates formed during the course of degradation as well as mineralization. The results obtained by various analytical tools were correlated for predicting the plausible mechanism of degradation and mineralization.

Experimental details

Ce^{3+} modified ZnO catalysts were synthesized by impregnating the pre-synthesized ZnO with Ce^{3+} ions. The details of the synthesis and the optical characterization of the synthesized powders by solid-state diffuse reflectance spectroscopy (DRS) as well as photoluminescence (PL) spectroscopy is discussed in our recent communication.[45] The assessment of the possible variation in the oxidation states of Ce^{3+} after being impregnated on hexagonal ZnO was investigated by X-ray photoelectron spectroscopy (XPS). X-ray Photoelectron Spectrometer (PHI 5000 VersaProbe II, ULVAC-PHI) recorded the XPS profiles of Ce^{3+} impregnated ZnO (Ce^{3+}@ZnO). The morphological and structural characterization of the impregnated photocatalysts was performed by FESEM and XRD analysis. The details about these techniques are available elsewhere.[45]

The photocatalytic activity of bare and Ce^{3+} impregnated ZnO in sunlight irradiation was performed by exposing 150 cm^3 of 30 ppm of respective MCP solution containing the optimized amount (100 mg) of respective catalyst. The procedure adopted for the optimization of catalyst for maximum degradation is detailed elsewhere.[46,47] Prior to sunlight exposure of the catalyst-MCP suspension was kept in the dark for the evaluation of adsorption. In sunlight exposure comparative studies, after a series experiments, it was realized that the important parameter is the intensity of light rather than the angle of incidence therefore all the experiments were performed in the sunlight illumination of $1000\pm100 \times 10^2$ lx and fixed period of the daylight. The progress of degradation process was monitored by drawing the samples after every 20 mins in the first hour and after 30 min in the next 1.5 h. In the next series of experiments, for most active catalyst, the concentration of MCP was increased to 50 ppm and performed the photocatalytic degradation studies by adopting the procedure described above. For the experiments with the mixtures of MCP isomers, a stock solution containing 17 ppm of each isomer was prepared by dilution method. The overall MCP content of the solution was 51 ppm. The mixture of MCP isomers was also subjected to similar procedure described above. After removing the catalyst by 0.20μm "Whatman" syringe filter, the

samples collected at various intervals were subjected to high performance liquid chromatography (HPLC), Ion chromatography (IC), TOC analysis and GC-MS analysis for estimating the decrease in phenolic substrate and formation of intermediates, estimation of anions in solution, removal of organic carbon and identification of intermediates, respectively. The details of the equipment and the parameters are given in Electronic Supplementary Information (ESI†).

Results and Discussion

Characterization of Ce^{3+} impregnated ZnO

The comparison of the PL analysis of the pure and Ce^{3+} loaded ZnO is presented in Fig. S1 (ESI†). The results are discussed in detail in our previous communication.[45] In the present study, the possible variations in the oxidation state of Ce during the synthesis were estimated by XPS analysis. The XPS survey scans of Ce^{3+} impregnated ZnO samples, where the peaks related to all the components are observable (Fig. 1). As expected, a decrease in the intensity of the peaks arising due to ZnO (Zn3p, Zn2p and O1s) and an increase for the peaks originated by the increasing surface density of Ce^{3+} was noticed. The C1s, O1s, Zn2p could be observed effortlessly however; the peaks of Ce4d and Ce3d because of low intensity are less prominent. For all the samples there was no shift in the position of C1s peaks that appeared at 285.1 eV. Fig. 2(a) and (b) shows the splitted Ce3d levels of 1% and 10% Ce^{3+} loaded ZnO. In 1% Ce^{3+} loading, the two Ce3d splitted levels appeared at 881.8 eV and 885.5 eV while for 10% Ce^{3+} loaded sample the same were shifted to lower binding energy of 880.6 eV and 884.4 eV due to the matrix effect. The obtained binding energy values, in accordance with the literature[48], confirmed the formation of surface Ce_2O_3 and Ce in +3 oxidation states. As shown in Fig. 2(c) and (d), the Zn2p3/2 peaks of 1% and 10% Ce^{3+} loaded samples appeared at the binding energies of 1022.4 and 1022.2 eV, respectively, which were as per literature values.[49] The appearance of additional shoulder in the fitting of Zn2p3/2 at 1020.22 eV (Fig. 2d) revealed the surface changes due to the presence of Zn^{2+}-O-Ce^{3+} type structures. The comparison of O1s peaks of 1% and 10% Ce^{3+} loaded ZnO is presented in Fig. 2 (e)

and (f). For both the samples the principal O1s peak arising due to surface Zn^{2+}-O^- appeared at around 530.9 eV while the shoulder, centered at 532.6 eV corresponds to oxygen deficient sites in ZnO matrix. The emergence of additional peak in O1s spectra of 10% Ce^{3+} impregnated ZnO sample at 529.4 eV corresponds to surface Ce_2O_3.[50,51]

The FESEM analysis, Figure 2, revealed no change in the morphology of ZnO rather even distribution of impregnating Ce^{3+} entities was noticed. With the increasing surface concentration, the deposition in overlaying layers, was observed that affected the sharpness of the edges of hexagonal ZnO. Also, no significant change in the particle size was observable.

The comparison of the XRD patterns of Ce^{3+} impregnated ZnO is presented in Figure 3. The main reflections appeared at 2θ values of 31.957, 34.603, 36.437, 47.711, 56.758, 63.012, 68.098, 69.236, 72.714, and 77.102 were corresponding to the hexagonal ZnO (JCPDS-36-1451). The growth of reflection at 2θ = 28.85º, with the increasing surface deposition of Ce^{3+} ions represented the hexagonal Ce_2O_3 (002) phase (JCPDS-23-1048). The other characteristic reflections of surface Ce_2O_3 were entrapped in intense ZnO reflections. The extrapolation of reflections at 2θ = 28.85º, revealed the crystallite size of ~6.6 nm for surface Ce_2O_3without the evidence of any change in oxidation state.

Photocatalytic degradation/mineralization of MCP isomers

The absorption of photons by the semiconductor particles leads to the generation of a cascade of reactive oxygen species (ROS) in the aqueous medium. The formation and population of these reactive entities entirely depend on the electrochemical potential of band edges and the pH of the system. The adsorbed water molecules are oxidized by valence band holes at the potential positive than +1.23V while the reduction of adsorbed/dissolved oxygen requires a minimum conduction band potential of -0.28V. The oxidation process leads to the formation of H^+ ions and hydroxyl radicals ($HO^\bullet$) whereas the reduction of adsorbed/dissolved oxygen generates superoxide anion radicals ($O_2^{\bullet-}$). The diffusion of these entities in the bulk initiates the formation of an additional stream of ROS that include $H_2O^\bullet$, H_2O_2, OH^- etc. In such a complex system, due to the presence

of a wide variety of reactive species, the extent of interaction of individual entity with the substrate is inconceivable. Similarly, in such a complex situation, it is hard to estimate the exact role of each reactive entity in the degradation/mineralization of the substrate. Recently, superoxide anion radicals ($O_2^{\bullet -}$) have replaced the hydroxyl radicals as the major oxidizing entities in photocatalytic degradation/mineralization processes. A complex route has been proposed for the generation of hydroxyl radicals. It has also been established that the formation of hydroxyl radicals is pH dependent and higher pH values favors the formation of superoxide anion radicals. The termination of the degradation activity in the absence of oxygen was used as supporting evidence in this regard.[41-44,52-56] As per our perception, in a photocatalytic degradation/mineralization process, the role of oxidizing species can be classified based on the careful identification of intermediates, estimation of total organic carbon removal and measurement of released ions.

Initially, the effect of various Ce^{3+} loadings (1%, 3%, 5% and 10%) on photocatalytic activity was estimated for the degradation/mineralization of 2-CP. The comparison of the HPLC degradation/mineralization profiles, showing the degradation of 2-CP and the formation of intermediates, in the sunlight exposure, over bare and Ce^{3+} impregnated ZnO is presented in Fig. 5 (a)-(e). All the Ce^{3+} loaded catalysts showed significantly higher activity for the degradation of 2-CP compared to bare ZnO. Although 2-CP was degraded in the presence of pure ZnO as well, however, the formation of intermediates was significantly higher. Whereas for Ce^{3+} impregnated catalysts, the simultaneous degradation of 2-CP substrate and removal of intermediates was observed. The percentage degradation of 2-CP as a function of sunlight exposure time is presented in Fig. 6 (a). Compared to ~40% degradation of 2-CP for bare ZnO, ~80%, ~77%, ~75% and ~86% of 2-CP substrate is removed in the presence of 1%, 3%, 5% and 10% Ce^{3+} loaded ZnO, respectively, in the initial 20 min of sunlight exposure. All the catalysts completely ($\geq$ 99.5%) degraded 2-CP substrate in 90 min of exposure while for bare ZnO ~95% of 2-CP was removed in 150 min. Compared to impregnated catalysts, a low TOC removal, as presented in Fig. 6 (b), was observed for bare ZnO. Compared to $\geq$ 90% TOC removal for all the catalysts in 150 min of exposure, 49% removal was observed for bare ZnO which was even lower than observed for Ce^{3+} impregnated catalysts in 20 min of exposure. The highest TOC removal of ~96% was observed for 10% Ce^{3+} loaded ZnO.

The rate profiles for the degradation and mineralization of 2-CP obtained by plotting ln (C_o/C) versus the sunlight exposure time are presented in Fig. 7 (a)-(b), where it can be inferred that the Langmuir-Hinshelwood kinetic model does not hold well for all the catalysts. For 1% and 10% Ce^{3+} loaded ZnO, during the degradation process, the rate of degradation exponentially increases with the decrease in the concentration of 2-CP substrate. A relatively better correlation was observed for pure, 3% and 5% Ce^{3+} loaded ZnO samples. Based on the results it can be generalized that in photocatalytic degradation processes the L-H kinetic model can only be applied for the catalysts with low or moderate activity.

The comparison of HPLC degradation profiles of 3-CP in standard (3-CP, 30 ppm) and exposed samples, on bare and Ce^{3+} impregnated ZnO is presented in Fig. S2 (ESI†). In the presence of bare ZnO, a low degradation (38% in 20 min) compared to Ce^{3+} impregnated catalysts (≥ 68% in 20 min) was observed. All the impregnated catalysts exhibited the ability to remove ~99.5% of 3-CP substrate in 120 min of sunlight exposure, however, the extent of degradation of 3-CP was lower than 2-CP. A similar behavior was observed in TOC removal (mineralization of intermediates). Compared to ~41% for bare ZnO, ~93% of organic carbon produced in 3-CP degradation was mineralized in 150 min of sunlight exposure.

As observed for 2-CP and 3-CP, the degradation of 4-CP in sunlight exposure over bare ZnO also generated a significant concentration of intermediates in the solution (Fig. S3, ESI†). A significantly higher degradation of 4-CP over Ce^{3+} impregnated ZnO catalyst as compared to bare ZnO was observed. Similarly, a high removal of TOC was also observed for all the catalysts. In 4-CP degradation, compared to ~36% for bare ZnO, ~97% of TOC removal was observed for 10% Ce^{3+} loaded catalyst in 150 min of sunlight exposure. However a lower degradation, compared to 2- and 3-CP, was observed under the similar conditions.

The comparison of the HPLC degradation profiles of 2-CP, 3-CP and 4-CP clearly elaborates that ZnO is capable of degrading MCP isomers in the natural sunlight, however, fails to carry out efficient mineralization (total organic carbon removal). On the

other hand, all Ce^{3+} impregnated catalysts showed excellent ability of simultaneous degradation and mineralization of MCP substrates. ZnO is a wide bandgap (3.1 eV) photocatalyst and can harvest only ≤ 5% of total incident photons (UV region) of the sunlight. In aqueous medium, the conduction band edge potential (-0.31 V) of ZnO is highly supportive for the reduction of dissolved oxygen to superoxide anion radicals. Additionally, pH_{ZPC} of 9.2 for ZnO also favors the formation of superoxide anion radicals in the photocatalytic degradation process. The negative aspect associated with ZnO is the high recombination of charge carriers. The high luminescence intensity of bare ZnO predicts the similar situation.[45] It is evident that the higher recombination rate of charge carriers *(e^--h^+)*, restricts the prolific use of excited states and fails to deliver the photo-excited electrons to adsorbed/dissolved O_2 thus generating fewer superoxide anion radicals compared to the number of absorbed photons. In the degradation process, for pure ZnO, the majority of the available superoxide anion radicals is consumed in the degradation of MCP substrates while very few are left in the system for interaction with intermediates thus affecting the mineralization ability significantly. The modification of ZnO surface by impregnating Ce^{3+} ions enhanced the photocatalytic degradation ability of ZnO tremendously led to significantly higher degradation and mineralization of MCP substrates. The varying extent of decrease in the luminescence intensity with respect to the concentration of Ce^{3+} confirmed at least the trapping capability of surface Ce^{3+} ions Figure S1 (ESI†). On the other hand, the significantly high simultaneous removal of MCP substrates and intermediates lead to the conclusion that a "trap" and "transfer" synergy exist between ZnO and impregnated Ce^{3+} ions. The impregnating Ce^{3+} ions bind with the ZnO surface oxygen to form "surface Ce_2O_3" nanostructures maintaining hexagonal geometry. The existence of surface Ce_2O_3 is also validated by XRD analysis. By the analysis of the HPLC degradation profiles of 2-CP, 3-CP and 4-CP, as presented in Fig. 3, S4 and S5, respectively, compared to 3% and 5% loadings, a noticeably high activity could be perceived for 1% and 10% Ce^{3+} loaded ZnO. However, a significantly high mineralization was observed for 10% Ce^{3+} loaded ZnO as compared to 1% loading that suggested that charge trapping and its transfer to the reductants is accomplished by more than one mechanism. It is proposed that at a lower surface density of Ce^{3+}, the photoexcited electrons are trapped by Ce^{3+} defects generated at the surface in the form of

Zn^{2+}-O-Ce^{3+} type structures. One possibility is the direct transfer of excited electrons from the conduction band of ZnO ($4s^0$) to the closely spaced 5d+4f orbital of Ce^{3+}. The presence of additional electron imparts instability to surface Ce^{3+} which is recuperated by the immediate transfer of electrons to adsorbed O_2 molecules that forms superoxide anion radicals ($O_2^{\bullet -}$) as presented in the pictorial representation given in the scheme I below.

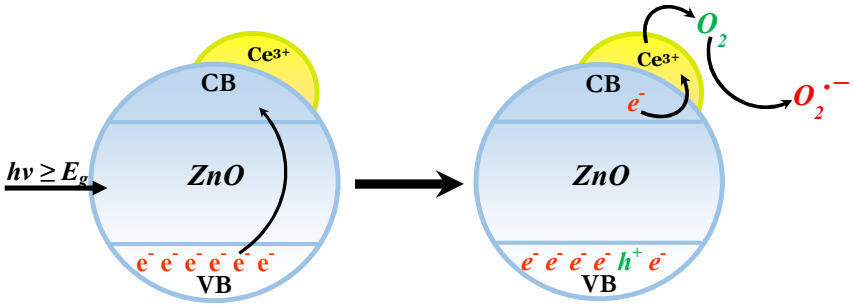

Scheme I: The plausible charge trapping and transfer mechanism for 1% Ce^{3+} loaded ZnO in sunlight exposure.

The layer by layer impregnation of Ce^{3+} with the increasing surface density hinders the charge transfer ability thus causes a decrease both in degradation and mineralization for 3% and 5% Ce^{3+} loaded ZnO catalysts. For 10% Ce^{3+} impregnated ZnO, the deposition of Ce^{3+} leads to the formation of surface composite or heterojunction of ZnO and Ce_2O_3. The formation of these heterostructures is well documented in the literature.[57-59] However, in this particular case, the structures are being formed by the layer by layer surface deposition of Ce^{3+} ions, the junction boundaries were difficult to identify even by HRTEM. The presence of additional absorption edge in the visible region absorption for 10% Ce^{3+} impregnated ZnO along with the bandgap edge of ZnO also supports the same.[45] Owing to two distinct absorption edges in the absorption spectra the two components of the composite, i.e. ZnO and Ce_2O_3 behave as independent photocatalysts under illumination and support each other in suppressing the unwanted charge carrier recombination. The substantial decrease in the luminescence intensity further augments this approach. ZnO has the valence band edge at +2.89 eV while Ce_2O_3 possesses the same at +1.90 eV. Similarly, the conduction band edges of ZnO and Ce_2O_3

lies at -0.31 and -0.5 eV, respectively. [60] Based on the suitability of their band edges, it can be predicted that both the components mutually facilitates each other through electrochemical allowed transitions to avoid the charge carrier recombination and enhance the lifetime of the excited states. Both ZnO and Ce_2O_3 have suitable band edges for the generation of superoxide radicals. In this consequence, the absorption of photons by any component of the composite results in the enhanced yield of $O_2^{\bullet-}$ radicals, hence resulting an increased activity for 10% Ce^{3+} loaded catalysts for the degradation of MCP isomers. The same is true for 3% and 5% Ce^{3+} impregnated catalysts, however, probably the amount of Ce_2O_3 that is formed is not sufficient enough to bring about any significant change rather a retarding effect was observed. The energetically favored transitions that dictate the enhanced activity of 10% Ce^{3+} loaded ZnO are pictorially explained in scheme II below.

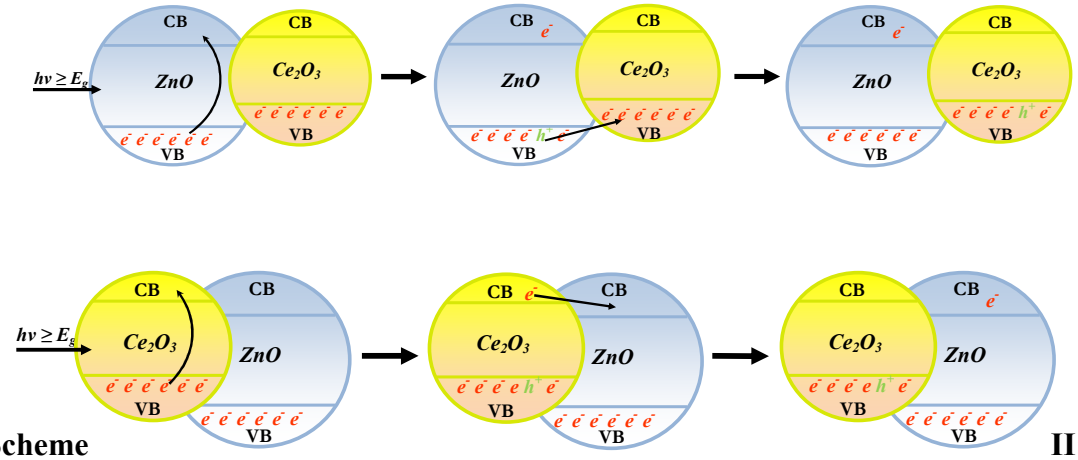

Scheme II: The plausible

The comparison of 2-CP, 3-CP and 4-CP degradation over 10% Ce^{3+} impregnated ZnO is presented in Fig. 8. The inset of the same figure gives an over overview of the TOC removal efficiency of the same catalyst for the three isomers. Due to the rapid degradation of 30 ppm of MCP substrates, it was hard to estimate the effect of the position of the chloro group in respective MCP isomers on degradation process. Additionally, the degradation of intermediates was extremely fast. To figure out the plausible role of the position of the Cl group in the degradation process and identification of intermediates, the experiments were performed with the higher concentration, 50 ppm, of MCP's in the presence of most active (10% Ce^{3+} loaded ZnO) catalyst keeping the

amount of the catalyst constant. The monitoring of the degradation process was carried out by drawing the samples at a regular interval of 30 min in the first two hours and 60 min in the final hour. The samples drawn after 30 min of sunlight exposure were extracted with dichloromethane for GC-MS analysis.

The HPLC degradation profiles of 2-CP, 3-CP and 4-CP (50 ppm) are presented in Fig. 9 (a)-(c). Due to the decrease in the oxidizing species to substrate ratio, the expected lower rate of degradation of MCP was observed. This relatively lower degradation/mineralization, compared to 30 ppm concentration, was found advantageous in the identification of intermediates, estimation of released ions, the influence of the position of chloride group on degradation process and predicting the degradation/mineralization mechanism. The comparison of the percentage degradation of 2-CP, 3-CP and 4-CP for 50 ppm concentration is presented in Fig. 10 (a), where a significant high degradation of 2-CP compared to 3-CP and 4-CP is observable. The variation in the time scale percentage degradation of MCP isomer revealed that the ease of degradation of respective MCP isomer depends on the position of attachment of Cl group with the aromatic system. The hindrance due to the stereo-chemical orientation of Cl group, inter and intra molecular hydrogen bonding, inductive and resonance effect may be the decisive factors in this regard. The more pronounced inductive effect and intra molecular hydrogen bonding in 2-CP makes it a soft target for interacting ROS as compared to 3-CP and 4-CP.[61] The low magnitude of the inductive effect due to the position of the Cl group in 3-CP and 4-CP results in the low degradation of these substrates. The inter-molecular hydrogen bonding leading to stabilized polymeric structure in 4-CP additionally contributes in the low degradation of 4-CP. Keeping in view the electron withdrawing nature of Cl group, the role of the inductive effect (-I) in generating the particular sites for the interaction of reactive species, cannot be ignored. The inset of Fig. 10 (a), shows the graphical evaluation of the rate of degradation of the three isomers. A linear relationship was observed in the degradation and sunlight exposure, which further strengthened the earlier comment that Langmuir-Hinshelwood kinetic model for pseudo first order reactions holds well for moderate reactions. The percentage mineralization (TOC removal) of the three substrates is presented in Fig. 10 (b), while the inset shows the rate of TOC removal. A trend similar to that observed in

the experiments with 30 ppm concentration was prevalent at higher concentration as well. The rate of TOC removal decreases with the decrease in the concentration of substrates as well as intermediates.

The Ion chromatography (IC) profiles of the three isomers are presented in Fig. S4 (ESI†), where the release of chloride ions in solution, corresponding to degradation, was observed. The release of Cl^- ions in substantial concentration revealed the involvement of superoxide anion radicals in the degradation of MCP isomers and clearly predicted that the degradation of MCP isomers is strictly associated with the displacement of Cl^-. The same is not achievable with the interaction of radical species. In MCP isomers, Cl atoms, being electronegative in nature, induce the positive charge on the attached carbon atom by its electron withdrawing effect thus generating a positive center for superoxide attack. The appearance of additional peaks evidenced further interaction of Cl^- ions with the reactive oxygen species especially superoxide anion radicals. The formation of ClO_2^-, ClO_3^- and ClO_4^- was identified and plotted in comparison to Cl^- ion for each isomer and presented in Fig. 11.

The degradation of each isomer was also investigated in the mixture of three isomers containing ~17 ppm of each isomer. The percentage degradation profiles of the three isomers are presented in Fig. 12, while the inset shows the HPLC profile for the simultaneous degradation of three isomers in the mixture at various time intervals. It was observed that the degradation pattern of the isomers in the mixture was similar to that of individual isomer, which depicted the selectivity of the oxidizing species for respective isomer.

In the HPLC analysis, 2-CP, 3-CP and 4-CP were eluted at 6.5, 8.1 and 7.8 min, respectively, under our experimental conditions described above. The common intermediates, having same retention time for the three isomers, appeared at the retention time of 2.05, 2.8 and 3.6 min. The intermediate at 4.6 min was common both for 2-CP and 3-CP and absent for 4-CP. An additional peak appeared at 3.3 min for 4-CP. The comparison of the HPLC chromatograms, recorded after 30 min of sunlight exposure, showing the retention time of the three substrates and intermediates is presented Fig. 13.

The above-mentioned samples were subjected to GC-MS analysis and the identification of respective isomer, in each analysis, was used as a marker. 2-CP, 3-CP and 4-CP were eluted at 11.408, 18.708 and 18.625 min, respectively. The comparison of GC chromatograms for the three isomers is presented in Fig. 14. Interestingly, the aliphatic oxygenates were identified as the major components of intermediates in GC-MS analysis. It is important to mention here that no chloro group bearing aromatic compound was identified for the three isomers. The compounds eluted at retention time 2.06 and 2.8 min in HPLC analysis were identified as $C_4H_8O_2$ (RT = 3.142 min.) and $C_6H_{12}O_2$ (RT = 4.042 min.) with mass numbers 88 and 116 g/mol, respectively. Another compound, in appreciable quantity, also having the mass number 88 g/mol was eluted at RT = 3.558 min and identified as $C_5H_{12}O$. The above-mentioned intermediates were found common in the degradation of isomers. Another common compound, common for both 2-CP and 3-CP was observed at 8.150 min and identified as $C_7H_{12}O_2$ with mass number 128 g/mol. $C_5H_{12}O_2$ (RT = 5.317 min) was observed only for 4-CP. A number of intermediates ranging from C_1-C_6 (formic acid, acetaldehyde, acetic acid, propanealdehyde etc.) were also observed beside the above-mentioned major intermediates. Moreover aliphatic intermediates, aromatic compounds like xylene and benzaldehyde was also spotted in the analysis. Captivatingly, the majority of identifying compounds were oxygenates that led to the assumption that the degradation of the MCP proceeds with the insertion of oxygen in the aromatic ring leading to the cleavage and formation of oxygenates.

In the present study, the theoretical and experimental evidences such as the conduction band edge position of ZnO (-0.31 eV), pH_{ZPC} of ZnO (9.2), rapid mineralization, release of chloride ions in solution and the presence of aliphatic oxygenated intermediates strongly supports the involvement of superoxide anion radicals in the degradation and mineralization process. Superoxide anion radicals ($O_2^{\bullet-}$), being negatively charged entities, seek positively charged locations to initiate the oxidation process rather than non-selective interaction as in case of hydroxyl radicals. The release of Cl^- ions in the solution supports the view that Cl bearing carbon in MCP's facilitates the superoxide attack.

Based on the above-mentioned experimental evidences, it can be inferred that the mineralization of MCP isomers is furnished mainly by the superoxide anion radicals. Although occurring simultaneously, the MCP isomers are degraded by the loss of aromaticity and the formation of oxygenated intermediates initially. The presence of chloro groups on the aromatic ring facilitates the degradation by imparting partial positive charge to the attached carbon atom. The intermediates, mostly polar oxygenates, are further interacted by superoxide anion radicals to mineralization. The identification of C_1, C_2 and C_3 products in GC-MS analysis revealed that larger (C_4-C_6) intermediates undergo further fragmentation before being mineralized. The presence of electronegative oxygen in the oxygenated intermediates facilitates the mineralization process. The plausible mechanism for the degradation of MCP isomers over 1% Ce^{3+} loaded ZnO and considering 4-CP as model substrate, can be further elaborated by the scheme III below.

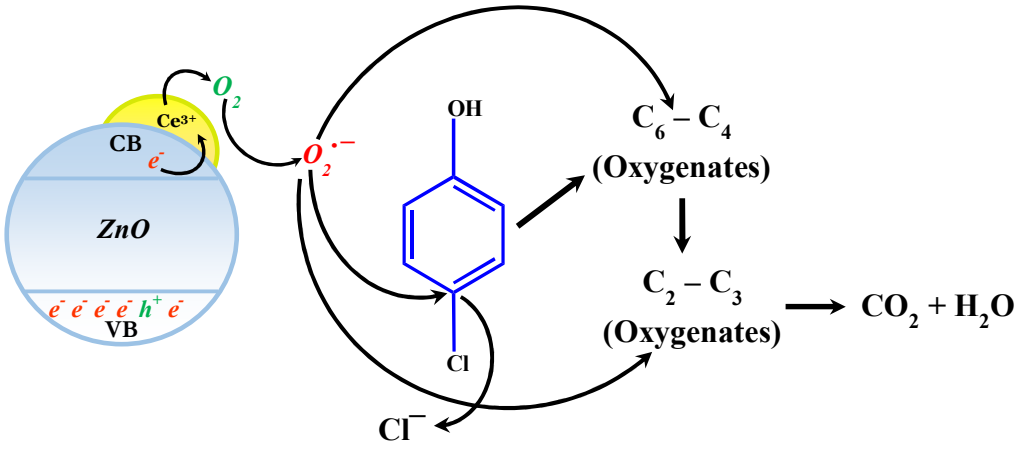

Scheme III: The anticipated mechanism of degradation/mineralization of 4-CP over 1% Ce^{3+} loaded ZnO.

The monitoring of released Zn^{2+} ions in the solution under sunlight illumination for bare and Ce^{3+} impregnated ZnO catalysts revealed ~13% corrosion of bare ZnO with respect to the weight of the loaded catalyst. Up to 5% Ce^{3+} loading an average of 4% photocorrosion was noticed while it was less than 1% for 10% Ce^{3+} loaded ZnO. The above-mentioned results are based on the measurement of Zn by ICP-OES after sunlight exposure of 150 min.

Conclusion

The surface presence of Ce^{3+} ions not only suppresses the unwanted e^{-}-h^{+} recombination but also improves the delivery of captured electron to reductants that enhances the photocatalytic activity substantially. The correlation of the data obtained by various analytical techniques revealed the superoxide anion radicals as major contributors in the mineralization process. The process of mineralization occurs in successive steps starting from the loss of aromaticity and formation of C_4-C_6 intermediates. The intermediates are further subjected to superoxide anion radical attack that leads to complete mineralization MCP isomers. The presence of chloro groups facilitates the mineralization process by imparting additional positive charge to the attached carbon atom. The study provides a base for sunlight photocatalytic mineralization of stable hazardous contaminants to complete detoxification. The surface presence of Ce^{3+} not only enhance the photocatalytic activity but significantly suppress the photocorrosion of ZnO.

Acknowledgements

Iqbal M.I. Ismail, A. Hameed and M. Aslam are greatly indebted to the Center of Excellence and Environmental Studies (CEES), King Abdulaziz University and Ministry of Higher Education (MoHE), Kingdom of Saudi Arabia, for their supports.

Notes and reference

1 M. Czaplicka, *Sci. Total Environ.*, 2004, **322**, 21–39.

2 M. Gomez, G. Matafonova, J. L. Gomez, V. Batoev and N. Christofi, *J. Hazard. Mater.,* 2009, **169**, 46–51.

3 A. O. Olaniran and E. O. Igbinosa, *Chemosphere*, 2011, **83**, 1297–1306.

4 M. Pera-Titus, V. García-Molina, M. A. Baños, J. Giménez and S. Esplugas, *Appl. Catal., B,* 2004, **47**, 219–256.

5 Y. Pi, L. Zhang and J. Wang, *J. Hazard. Mater.*, 2007, **141**, 707–712.

6 J. Krýsa, G. Waldner, H. Měšťánková, J. Jirkovský and G. Grabner, *Appl. Catal. B: Environ.*, 2006, **64**, 290–301.

7 M. Czaplicka, *J. Hazard. Mater.*, 2006, **134**, 45–59.

8 J. R. Bolton and S. R. Cater, Homogeneous photo-degradation of pollutants in contaminated water; an introduction, R. G. Zepp, G. R. Helz, D.G. Crosby (Eds.), Aquatic and surface photochemistry, Lewis Publisher, Boca Raton, FL, 1994, 467–690.

9 F. Hodin, H. Borén and A. Grimvall, *Water Sci. Technol*., 1991, **24**, 403–410.

10 N. Wang, X. Li, Y. Wang, X. Quan and G. Chen, *Chem.Eng. J.,* 2009, **146**, 30–35.

11 M. F. Sze and G. McKay, *Water Res.,* 2012, **46**, 700-10.

12 L. M. Cotoruelo, M. D. Marqus, J. Rodrguez-Mirasol, T. Cordero and J. J. Rodrguez, *Ind. Eng. Chem. Res.*, 2007, **46**, 2853-2860.

13 V. C. Srivastava, M. M. Swamy, I. D. Mall, B. Prasad and I. M. Mishra, *Colloids Surf., A* 2006, **272**, 89-104.

14 D. Chen and A. K. Ray, *Appl. Catal. B: Environ*., 1999, **23**, 143–157

15 J. L. Wang and Y. Qian, *Chemosphere*, 1999, **38,** 3109–3114.

16 U. I. Gaya and A. H. Abdullah, *J. Photochem. Photobiol. C: Photochem. Rev.*, 2008, **9**, 1-12.

17 M. D. Murcia, M. Gomez, E. Gomez, J. L. Gomez and N. Christofi, *WASET,* 2009, **31,** 245-249.

18 M. H. Priya and G. Madras, *Ind. Eng. Chem. Res.*, 2006, **45**, 482-486.

19 M. H. Hernández-Alonso, F. Fresno, S. Suárez, and J. M. Coronado, *Energy Environ. Sci.*, 2009, **2,** 1231-1257.

20 S. Rehman, R. Ullah, A. M. Butt and N. D. Gohar, *J. Hazard. Mater.*, 2009, **170**, 560-569.

21 A. Fujishima, T. N. Rao and D. A. Tryk, *J. Photochem. Photobiol. C: Photochem. Rev*., 2000, **1,** 1–21.

22 Q. U. Jiuhui, *J. Environ. Sci.*, 2008, **20,** 1–13.

23 D. S. Bhatkhande, V. G. Pangarkar and A. A. C. M. Beenackers, *J. Chem. Technol. Biotechnol.*, 2002, **77,** 102–116.

24 C. Lettmann, H. Hinrichs and W. F. Maier, *Angew. Chem. Int. Ed*., 2001, **40**, 3160–3164.

25 M. A. Lazar, S. Varghese and S. S. Nair, *Catalysts*, 2012, **2**, 572-601.

26 A. Mills, R.H. Davies and D. Worsley, *Chem. Soc. Rev.*, 1993, **22,** 417-425.

27 M. N. Chong, B. Jin, C. W. K. Chow and C. Saint, *Water Res.*, 2010, **44**, 2997–3027.

28 O. Carp, C. L. Huisman and A. Reller, *Prog. Solid State Chem.*, 2004, **32,** 33–177.

29 K. Vinodgopal, U. Stafford, K. A. Gray and P. V. Kamat, *J. Phys. Chem.*, 1994**, 98,** 6797–6803.

30 W. S. Jenks, X. Li and J. W. Cubbage, *J. Org. Chem.* 1999, **64**, 8525-8536.

31 X. Li, J. W. Cubbage, T. A. Tetzlaff and W. S. Jenks, *J. Org. Chem.*, 1999**, 64***,* 8509–8524.

32 K. Okamoto, Y. Yamamoto, H. Tanaka and M. Tanaka, *Bull. Chem. Soc. Jpn.***,** 1985, **58**, 2015-2022.

33 K. Okamoto, Y. Yamamoto, H. Tanaka and A. Itaya, *Bull Chem. Soc. Jpn.*, 1985, **58,** 2023-2028.

34 Z. Ai, P. Yang and X. Lu, *J. Hazard. Mater.*, 2005, **124,** 147-152.

35 J. M. Tseng and C. P. Huang, *Water Sci. Tech.*, 1991, **23,** 377-387.

36 M. Czaplicka, *J. Hazard. Mater.*, 2006, **134,** 45–59.

37 P. Boule, C. Guyon and J. Lemaire, *Chemosphere*, 1982, **11,** 1179–1188.

38 A. Daniela, C. Cezar, D. Brândusa and T. Carmen, *Environ. Eng. Manag. J.*, 2010, **9,** 7-16.

39 W. S. Jenks, X. Li, J. W. Cubbage and T. A. Tetzlaff, *J. Org. Chem.*, 1999, **64,** 8509-8524.

40 Y. Y. Wu, H. Yan and P. Yang, *Top. Catal.*, 2002, **19,** 197-202.

41 M. Law, L. E. Greene, J. C. Johnson, R. Saykally and P. Yang, *Nat. Mater.*, 2005, **4,** 455-459.

42 M. Law, L. E. Greene, A. Radenovic, T. Kuykendall, J. Liphardt and P. Yang, *J. Phys. Chem. B*, 2006, **110,** 22652-22663.

43 A. Hameed, T. Montini, V. Gombac and P. Fornasiero, *Photochem. Photobiol. Sci.*, 2009, **8,** 677-682.

44 A. Hameed, V. Gombac, T. Montini, L. Felisari and P. Fornasiero, *Chem. Phys. Lett.*, 2009, **483,** 254-261.

45 I. M. I. Ismail, M. Aslam, T. Almeelbi, S. Chandrasekarana and A. Hameed, *RSC Adv.*, 2014, **4,** 16043–16046.

46 M. Aslam, I. M. I. Ismail, S. Chandrasekaran and A. Hameed, *J. Hazard. Mater.*, 2014, **276,** 120-128.

47 A. Hameed, M. Aslam, I. M. I. Ismail, S. Chandrasekaran, M. W. Kadi and M. A. Gondal, *Appl. Catal., B.* 2014, **160-161,** 227-239.

48 A. M. Salvi, F. Decker, F. Varsano and G. Speranza, *Surf. Interface Anal.*, 2001, **31**, 255–264.

49 X. Q. Wei, B. Y. Man, M. Liu, C. S. Xue, H. Z. Zhuang and C. Yang, *Physica B: Condensed Matter*, 2007, **388,** 145-152.

50 T. L. Barr, C. G. Fries, F. Cariati, J. C. J. Bart and N. Giordano, *J. Chem. Soc. Dalton Trans.,* 1983, 1825–1829.

51 V. J. Ferreira, P. Tavares, J. L. Figueiredo and J. L. Faria, *Catal. Commun.*, 2013, **42,** 50-53.

52 B. G. Kwon and J. Yoon, *Bull. Korean Chem. Soc.* 2009, **30,** 667-670.

53 P. Pichat, *Photocatalysis and Water Purification: From Fundamentals to Recent Applications*, 1st edn, Wiley-VCH Verlag, Germany, 2013.

54 T. Hirakawa and Y. Nosaka, *Langmuir*, 2002, **18,** 3247–3254.

55 M. A. Henderson, *Surf. Sci. Rep.* 2011, **66**, 185–297.

56 B. H. J. Bielski, D. E. Cabelli and R. L. Arudi, *J. Phys. Chem. Ref. Data*, 1985, **14**, 1041–1100.

57 X. Wang, S. Shen, S. Jin, J. Yang, M. Li, X. Wang, H. Han and C. Li, *Phys. Chem. Chem. Phys.*, 2013, **15**, 19380-19386.

58 X. Wang, Q. Xu, M. Li, S. Shen, X. Wang, Y. Wang, Z. Feng, J. Shi, H. Han and C. Li, *Angew. Chem. Int. Ed.*, 2012, **51**, 13089-13092.

59 H. G. Kim, P. H. Borse, W. Choi and J. S. Lee , *Angew. Chem. Int. Ed.*, 2005, **44**, 4585- 4589.

60 Y. Xu and M. A. A. Schoonen, *Am. Mineral.*, 2000, **85,** 543-556.

61 A. Maldotti, A. Molinari and R. Amadelli, *Chem. Rev.*, 2002, **102**, 3811–3836.

Figure Captions

Fig. 1. The comparison of the XPS survey scans of 1%, 3%, 5% and 10% Ce^{3+} impregnated ZnO.

Fig. 2. The comparison of the core shell XPS spectra of Ce3d (a, b), Zn 2p3 (c, d) and O1s (e, f) in 1% and 10% Ce^{3+} impregnated ZnO respectively.

Fig. 3. High resolution (120,000×) FESEM images of (a) 1%Ce^{3+}@ZnO (b) 3%Ce^{3+}@ZnO (c) 5%Ce^{3+}@ZnO and (d) 10%Ce^{3+}@ZnO

Fig. 4. (a) The comparison of the XRD of pure (black), 1%Ce^{3+}@ZnO (red), 3%Ce^{3+}@ZnO (green), 5%Ce^{3+}@ZnO (blue) and 10%Ce^{3+}@ZnO (pink) (b) the XRD patterns of pure (black) with Ce^{3+} impregnated ZnO in $2\theta = 20^{\circ}$ and $2\theta = 20^{\circ}$ range showing the growth of Ce_2O_3 with increasing concentration of Ce^{3+}.

Fig. 5. The comparison of HPLC degradation profiles of 2-CP (30 ppm) over (a) pure ZnO (b) 1%Ce^{3+}@ZnO (c) 3% Ce^{3+}@ZnO (d) 5% Ce^{3+}@ZnO and (e) 10% Ce^{3+}@ZnO

Fig. 6. The comparison of the percentage degradation of 2-CP (30 ppm) in sunlight exposure (1000±100 x 10^2 lx) in the aqueous suspension (100 mg/150 ml) over 1%, 3%, 5% and 10% Ce^{3+}@ZnO. The inset shows the TOC removal as a function of sunlight exposure time.

Fig. 7. The rate profile of (a) 2-CP (30 ppm) degradation (b) 2-CP mineralization in sunlight exposure (1000±100 x 10^2 lx) in the aqueous suspension (100 mg/150 ml) over 1%, 3%, 5% and 10% Ce^{3+}@ZnO.

Fig. 8. The comparison of the percentage degradation 2-CP, 3-CP and 4-CP, 30 ppm, in sunlight exposure (1000±100 x 10^2 lx) in the aqueous suspension (100 mg/150 ml) over 10% Ce^{3+}@ZnO. The inset shows the time scale TOC removal of the three chlorophenols isomers.

Fig. 9. The comparison of the degradation profiles of (a) 2-CP (b) 3-CP and (c) 4-CP, 50 ppm, in sunlight exposure (1000±100 x 10^2 lx) in the aqueous suspension (100 mg/150 ml) over 10% Ce^{3+}@ZnO. The inset shows the time scale TOC removal of the three chlorophenols isomers. Arrows on each figure mark the major intermediates

Fig. 10. The comparison of (a) the percentage degradation of 2-CP, 3-CP and 4-CP, 50 ppm, (b) percentage mineralization in sunlight exposure (1000±100 x 10^2 lx)

in the aqueous suspension (100 mg/150 ml) over 10% Ce^{3+}@ZnO. The inset shows the plots of ln (C_o/C) versus time. The inset of (a) and (b) shows the graphical evaluations of rate of degradation and mineralization respectively.

Fig. 11. The comparison of the release of various ions during the course of chlorophenols (50 ppm) isomers degradation and mineralization a) 2-CP b) 3-CP and c) 4-CP

Fig. 12. The comparison of the percentage degradation of 2-CP, 3-CP and 4-CP in the mixture of three isomers (17 ppm each) in sunlight exposure (1000±100 x 10^2 lx) in the aqueous suspension (100 mg/150 ml) over 10% Ce^{3+}@ZnO. The inset shows the HPLC degradation profile of three isomers in the mixture.

Fig. 13. The comparison of (a) HPLC chromatograms of 2-CP, 3-CP and 4-CP, 50 ppm, after 30 min of sunlight exposure (1000±100 x 10^2 lx) in the aqueous suspension (100 mg/150 ml) over 10% Ce^{3+}@ZnO. The retention times of the substrates and major intermediates are presented on the figure.

Fig. 14. GC-MS profiles of 2-CP, 3-CP, 4-CP and their mixture thereof over 10% Ce^{3+} impregnated ZnO after 30 min of sunlight exposure. The inset shows the separation of 3-CP and 4-CP peaks.

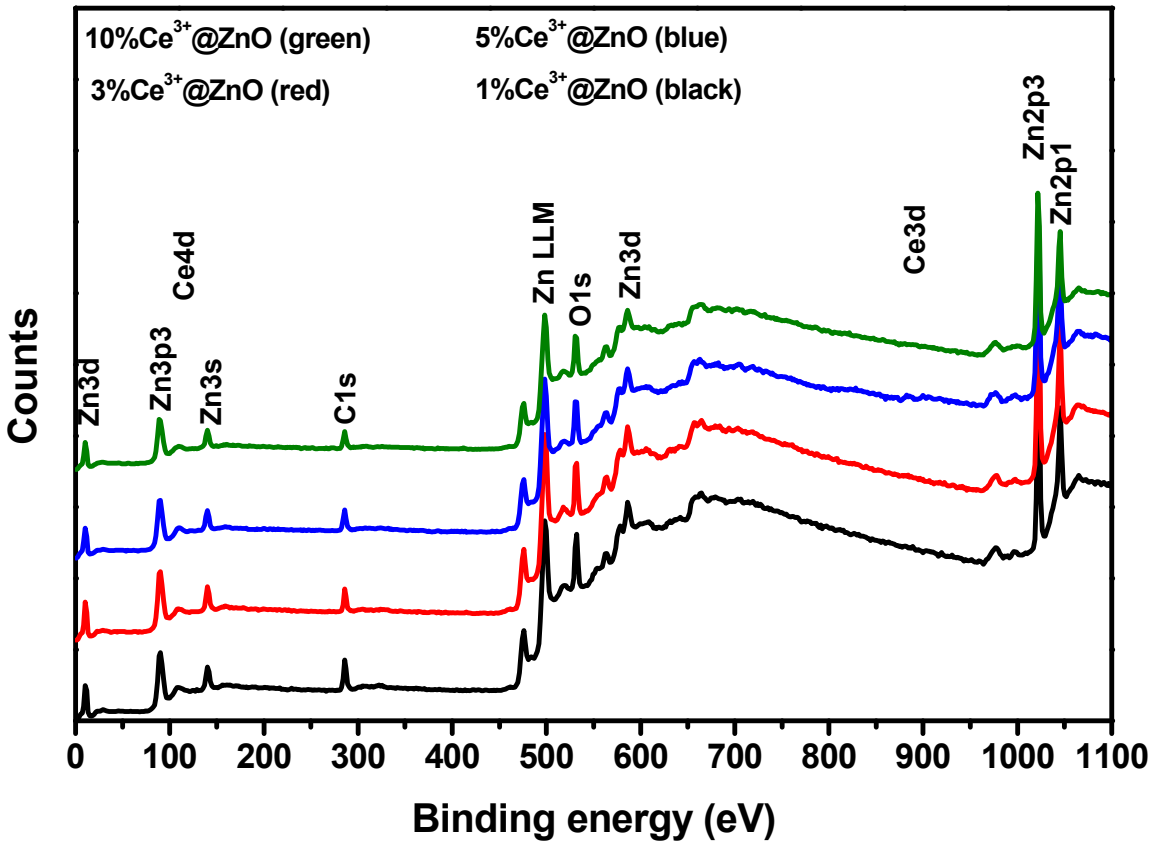

Fig. 1. The comparison of the XPS survey scans of 1%, 3%, 5% and 10% Ce^{3+} impregnated ZnO.

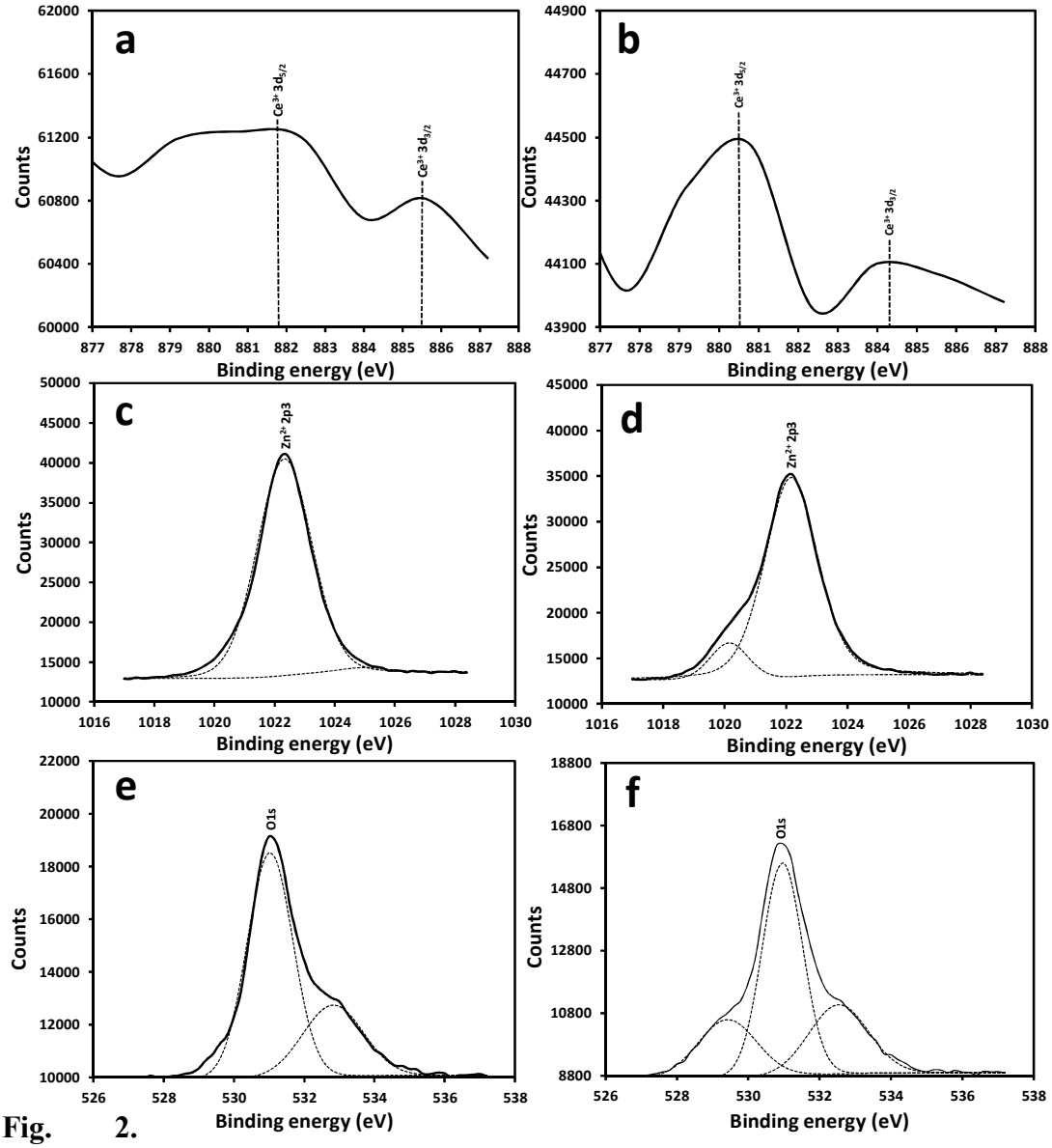

Fig. 2. The comparison of the core shell XPS spectra of Ce3d (a, b), Zn 2p3 (c, d) and O1s (e, f) in 1% and 10% Ce^{3+} impregnated ZnO, respectively.

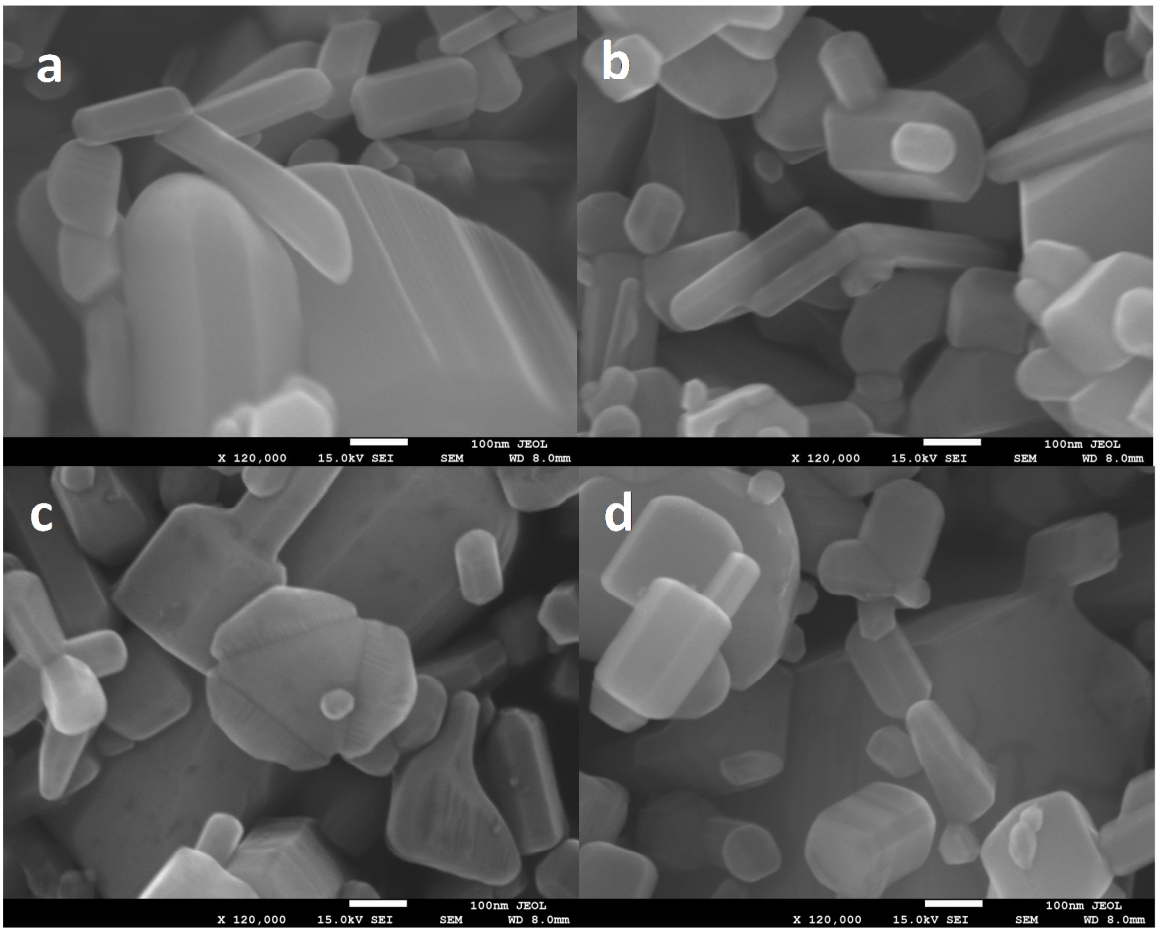

Fig. 3. High resolution (120,000×) FESEM images of (a) 1%Ce^{3+}@ZnO (b) 3%Ce^{3+}@ZnO (c) 5%Ce^{3+}@ZnO and (d) 10%Ce^{3+}@ZnO.

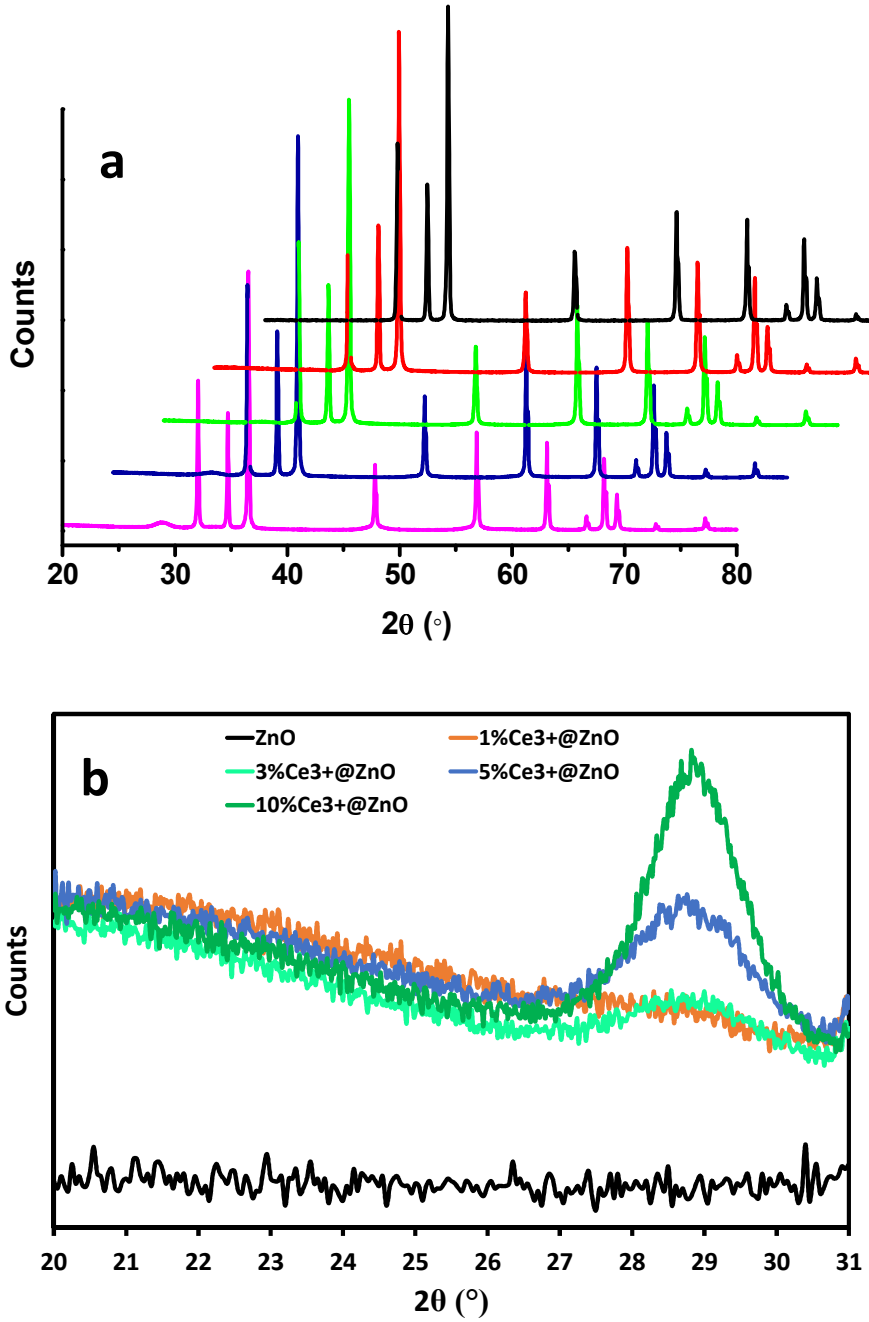

Fig. 4. (a) The comparison of the XRD of pure (black), 1%Ce^{3+}@ZnO (red), 3%Ce^{3+}@ZnO (green), 5%Ce^{3+}@ZnO (blue) and 10%Ce^{3+}@ZnO (pink) (b) the XRD patterns of pure (black) with Ce^{3+} impregnated ZnO in $2\theta = 20^{\circ}$ and $2\theta = 20^{\circ}$ range showing the growth of Ce_2O_3 with increasing concentration of Ce^{3+}.

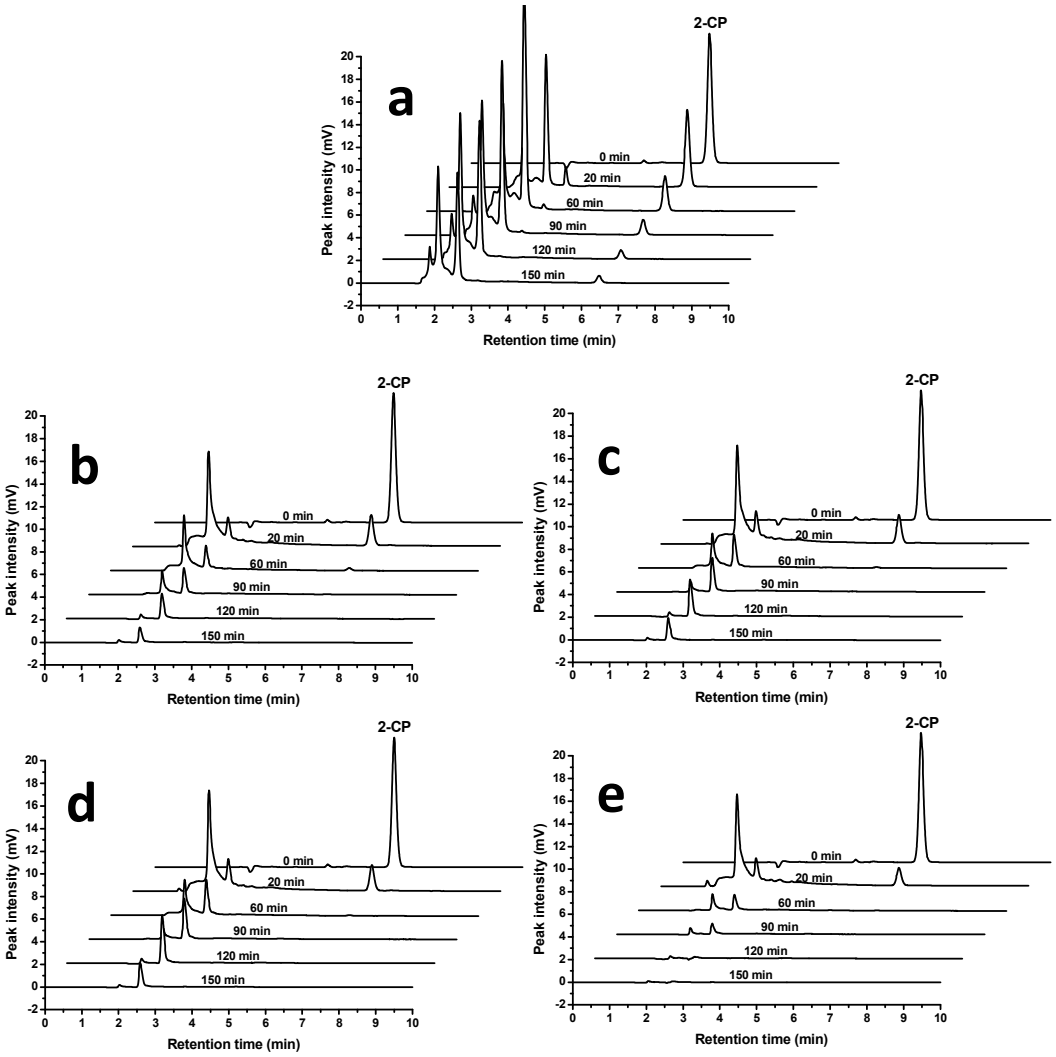

Fig. 5. The comparison of HPLC degradation profiles of 2-CP (30 ppm) over (a) pure ZnO (b) 1%Ce^{3+}@ZnO (c) 3% Ce^{3+}@ZnO (d) 5% Ce^{3+}@ZnO and (e) 10% Ce^{3+}@ZnO

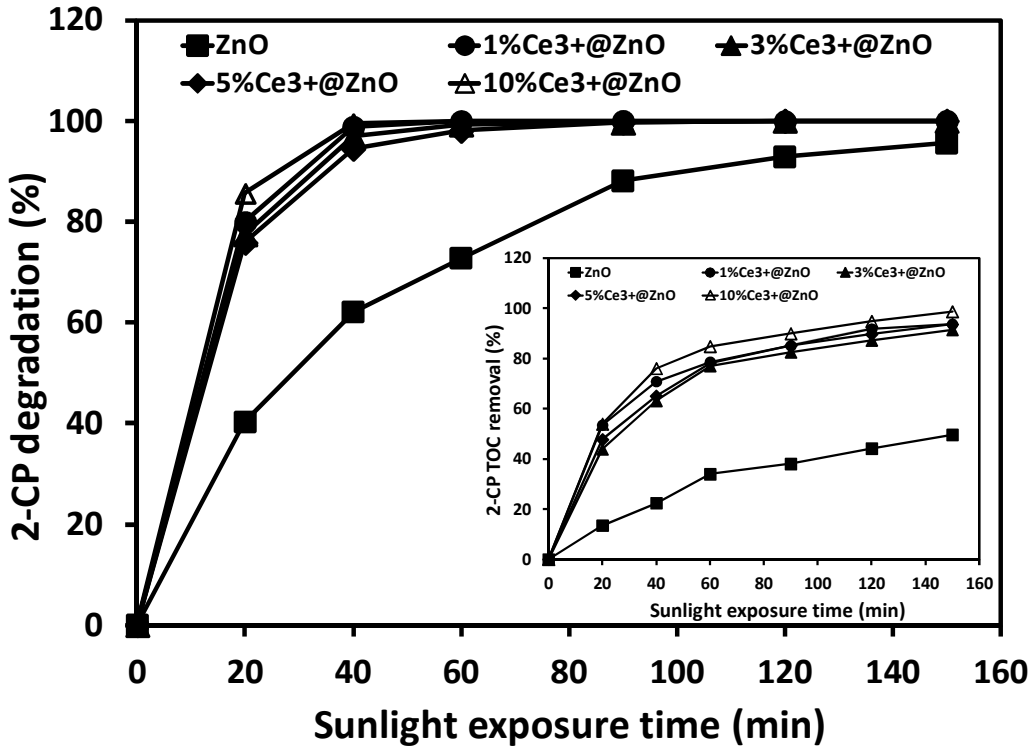

Fig. 6. The comparison of the percentage degradation of 2-CP (30 ppm) in sunlight exposure (1000±100 × 10^2 lx) in the aqueous suspension (100 mg/150 ml) over 1%, 3%, 5% and 10% Ce^{3+}@ZnO. The inset shows the TOC removal as a function of sunlight exposure time.

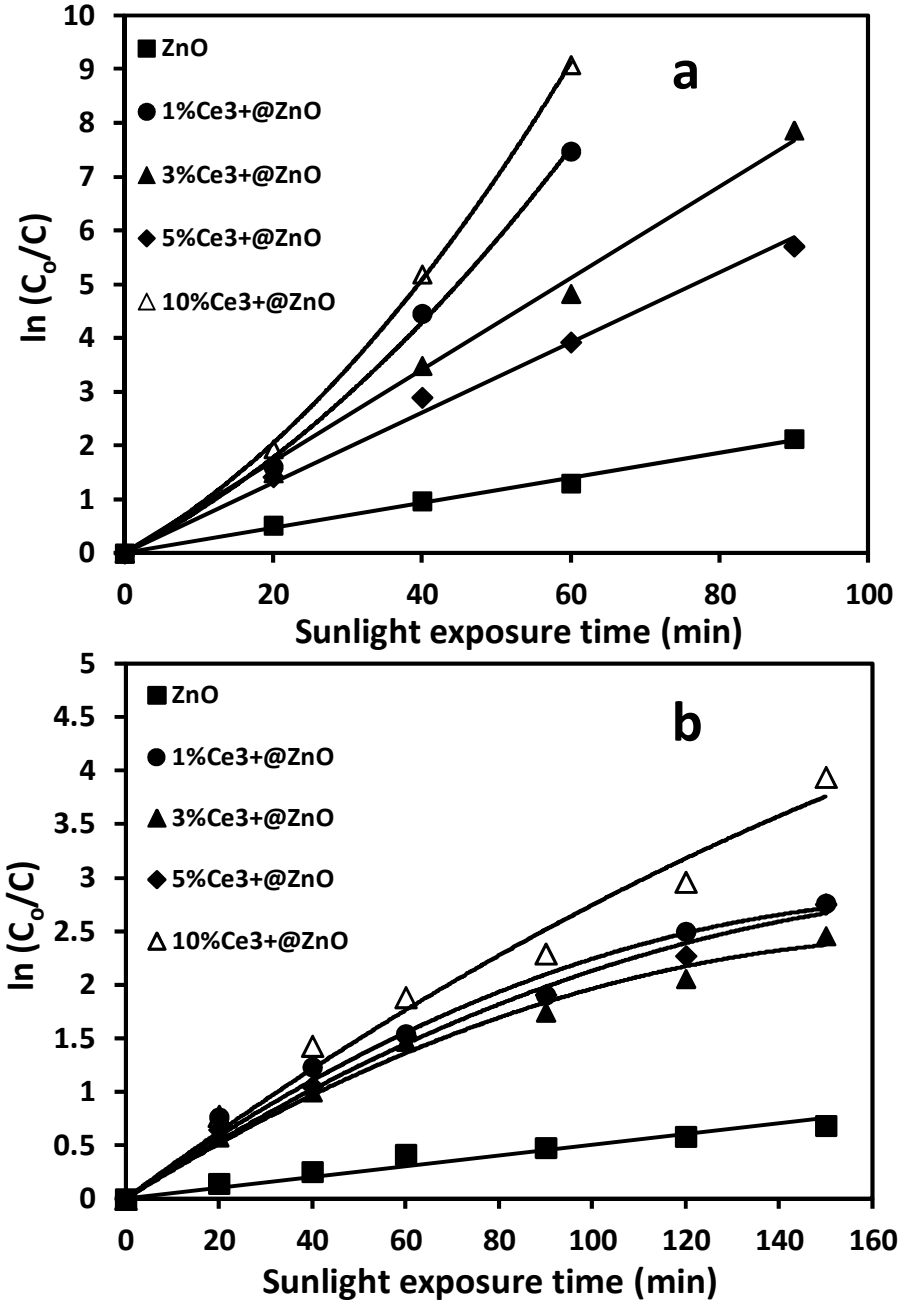

Fig. 7. The rate profile of (a) 2-CP (30 ppm) degradation (b) 2-CP mineralization in sunlight exposure (1000±100 × 10^2 lx) in the aqueous suspension (100 mg/150 ml) over 1%, 3%, 5% and 10% Ce^{3+}@ZnO.

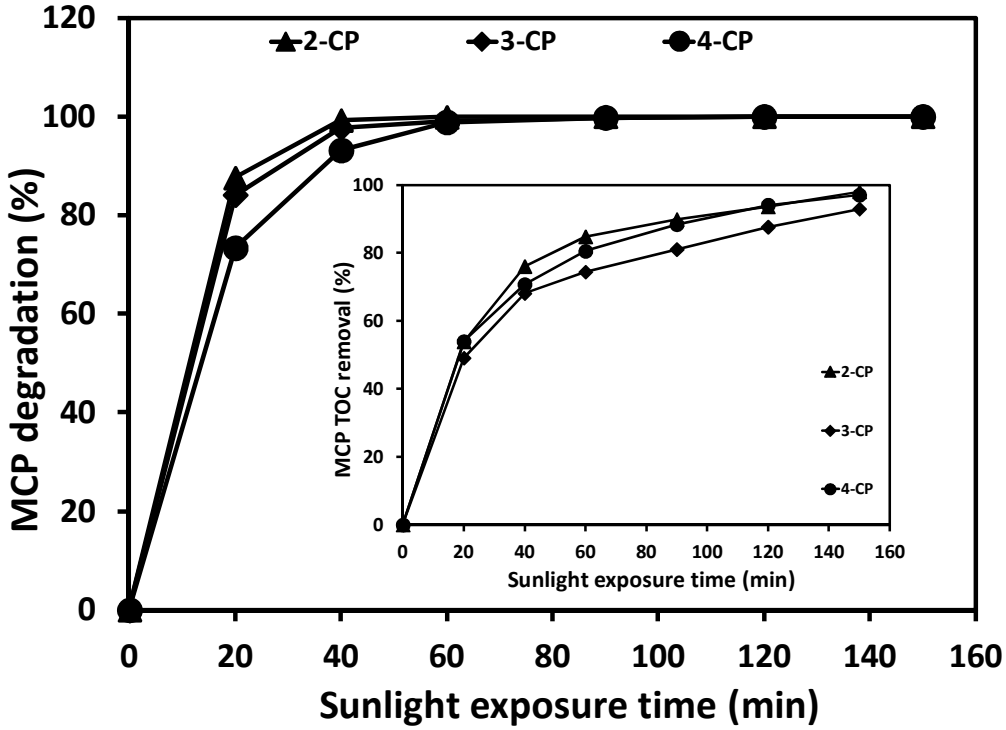

Fig. 8. The comparison of the percentage degradation 2-CP, 3-CP and 4-CP, 30 ppm, in sunlight exposure (1000±100 × 10^2 lx) in the aqueous suspension (100 mg/150 ml) over 10% Ce^{3+}@ZnO. The inset shows the time scale TOC removal of the three chlorophenols isomers.

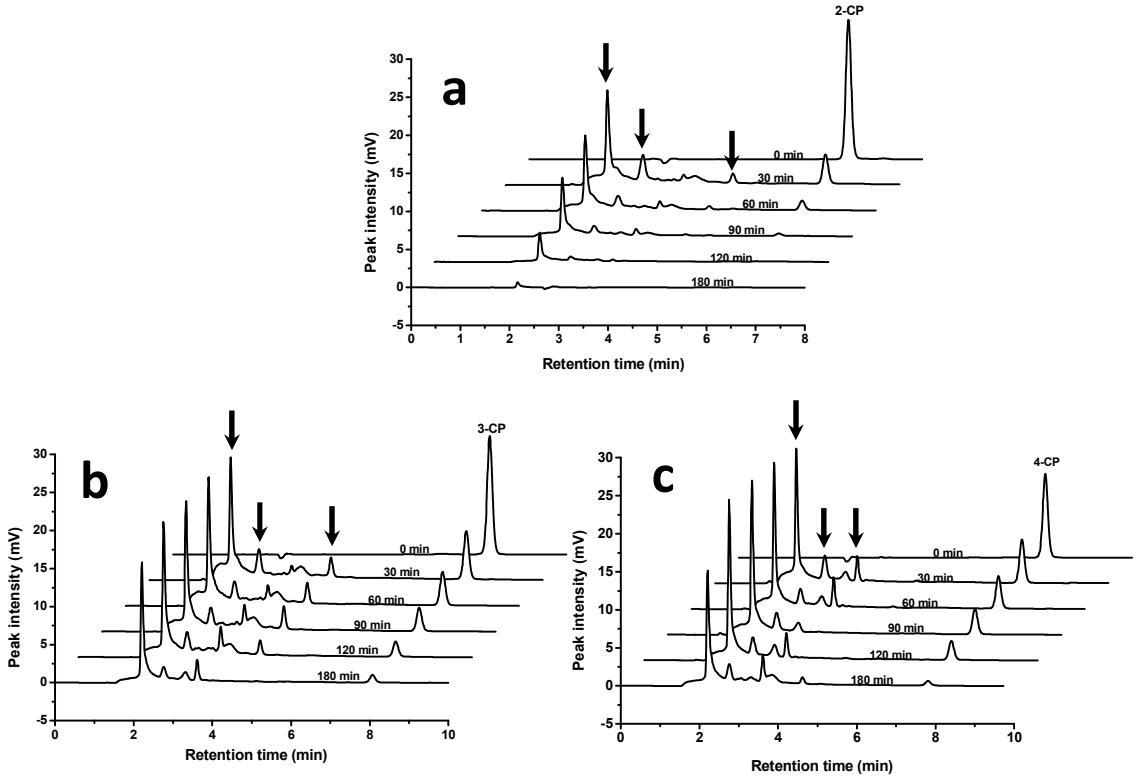

Fig. 9. The comparison of the degradation profiles of (a) 2-CP (b) 3-CP and (c) 4-CP, 50 ppm, in sunlight exposure (1000±100 × 10^2 lx) in the aqueous suspension (100 mg/150 ml) over 10% Ce^{3+}@ZnO. The inset shows the time scale TOC removal of the three chlorophenols isomers. Arrows on each figure mark the major intermediates

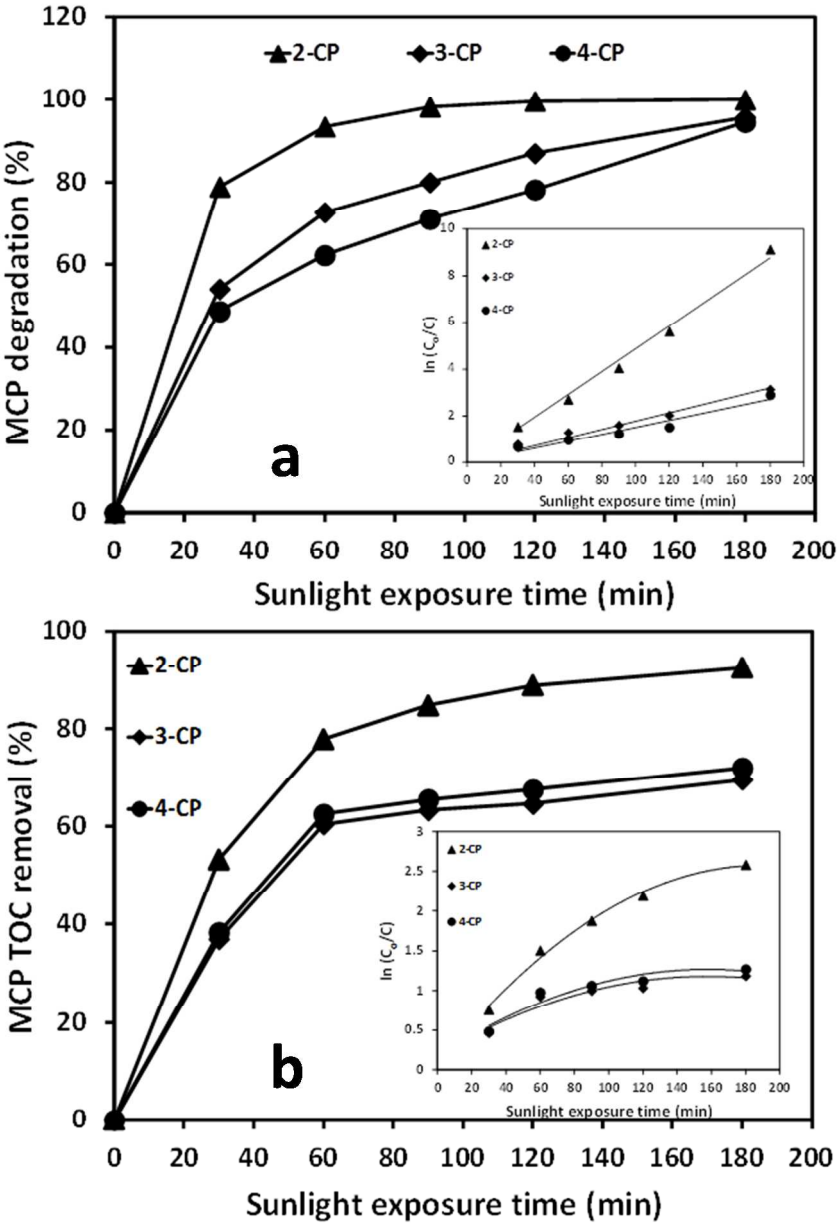

Fig. 10. The comparison of (a) the percentage degradation of 2-CP, 3-CP and 4-CP, 50 ppm, (b) percentage mineralization in sunlight exposure (1000±100 × 10^2 lx) in the aqueous suspension (100 mg/150 ml) over 10% Ce^{3+}@ZnO. The inset shows the plots of ln (C_o/C) versus time. The inset of (a) and (b) shows the graphical evaluations of rate of degradation and mineralization respectively.

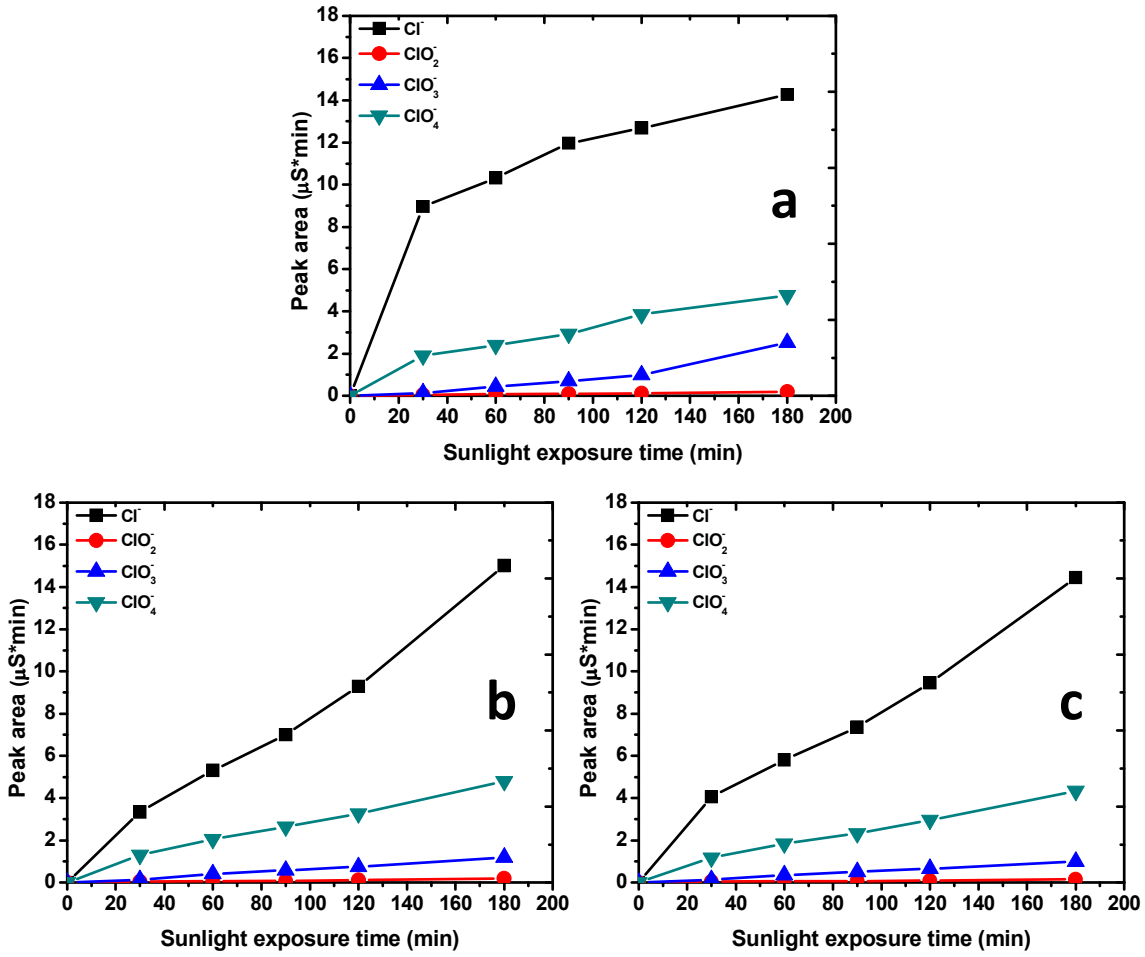

Fig. 11. The comparison of the release of various ions during the course of chlorophenols (50 ppm) isomers degradation and mineralization (a) 2-CP (b) 3-CP and (c) 4-CP.

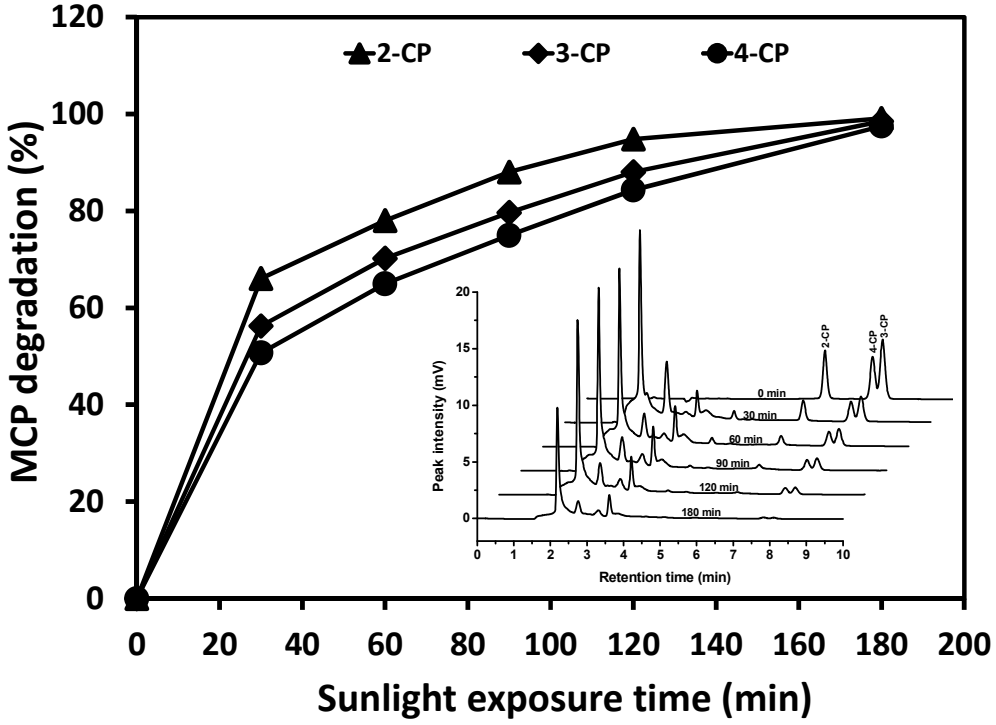

Fig. 12. The comparison of a) the percentage degradation b) the plots of $\ln(C_o/C)$ versus time for the degradation of 2-CP, 3-CP and 4-CP in the mixture of three isomers (17 ppm each) in sunlight exposure ($1000\pm100 \times 10^2$ lx) in the aqueous suspension (100 mg/150 ml) over 10% Ce^{3+}@ZnO. The inset shows the HPLC degradation profile of three isomers in the mixture.

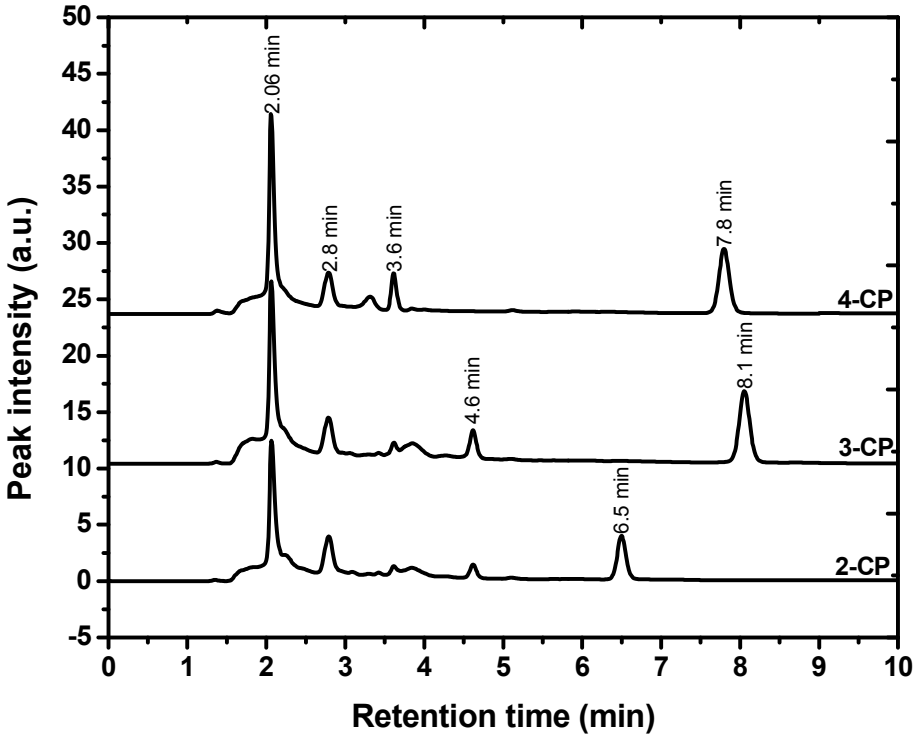

Fig. 13. The comparison of HPLC chromatograms of 2-CP, 3-CP and 4-CP, 50 ppm, after 30 min of sunlight exposure (1000±100 × 10^2 lx) in the aqueous suspension (100 mg/150 ml) over 10% Ce^{3+}@ZnO. The retention times of the substrates and major intermediates are presented on the figure.

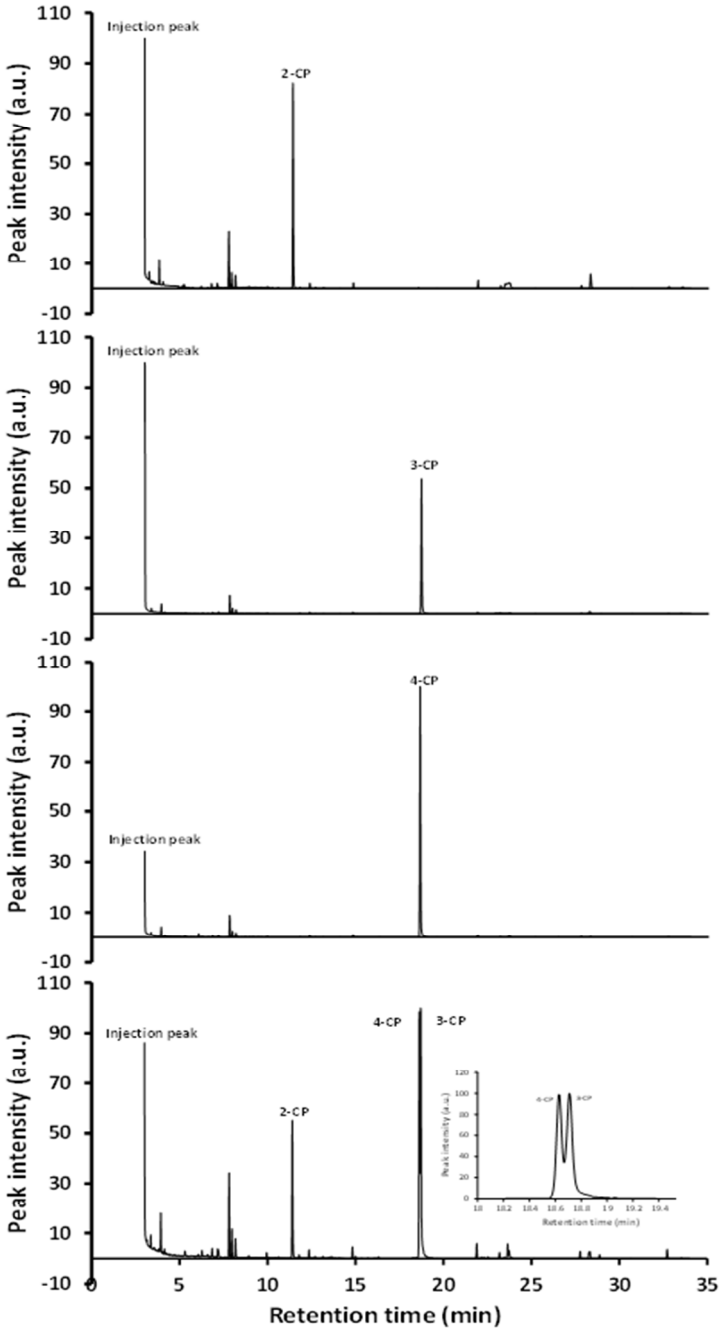

Fig. 14. GC-MS profiles of 2-CP, 3-CP, 4-CP and their mixture thereof over 10% Ce^{3+} impregnated ZnO after 30 min of sunlight exposure. The inset shows the separation of 3-CP and 4-CP peaks.